# Electronic and Structural Instabilities in $GaV_4S_8$ and $GaMo_4S_8$

Regina Pocha and Dirk Johrendt*

*Institut für Anorganische Chemie und Strukturchemie II, Heinrich-Heine-Universität Düsseldorf, Universitätsstrasse 1, D-40225 Düsseldorf, Germany*

Rainer Pöttgen†

*Department Chemie, Ludwig-Maximilians-Universität München, Butenandtstrasse 5-13 (Haus D), D-81377 München, Germany*

*Received May 29, 2000. Revised Manuscript Received July 3, 2000*

$GaV_4S_8$ was prepared by direct heating of the elements at 1123 K. The crystal structures were refined from single-crystal data at room temperature (*RT*-$GaV_4S_8$, $GaMo_4S_8$-type, $F\bar{4}3m$, $a = 9.661(1)$ Å, $Z = 4$) and by the Rietveld method at 20 K (*LT*-$GaV_4S_8$, $R3m$, $a = 6.834(1)$ Å, $\alpha_{rh} = 59.66(2)°$, $Z = 1$). Magnetic measurements show weak paramagnetism with a temperature-dependent magnetic moment between $1.5\mu_B$(50 K) and $1.9\mu_B$(300 K) compatible with one unpaired electron per $V_4$ cluster. Ferromagnetic ordering was detected below $T_C = 10$ K. DC electrical conductivity measurements between 30 and 320 K reveal semiconducting behavior. $GaV_4S_8$ undergoes a structural phase transition at 38 K from cubic to rhombohedral symmetry, as known for $GaMo_4S_8$, but with an opposite change of the rhombohedral angle $\alpha_{rh}$. This behavior is explained by self-consistent band structure calculations and simple cluster orbital schemes for $GaV_4S_8$ in comparison with $GaMo_4S_8$. The results prove that the directions of the structural deformations are determined by orbital interactions and depend on the electron count in the tetrahedral metal cluster units.

## Introduction

Chalcogenides with the $GaMo_4S_8$ structure are built up by heterocubane-like $[M_4X_4]^{n+}$ cubes (M = Mo, Re, V, Nb, Ta; X = S, Se, Te) and $[AX_4]^{n-}$ tetrahedra (A = Ga, Ge), arranged in a NaCl manner.[1−5] This structure is frequently described as a cation deficient spinel $A_{0.5}\square_{0.5}M_2X_4$, where the ordering of the tetrahedral sites reduces the symmetry from $Fd\bar{3}m$ to $F\bar{4}3m$. At the same time, the M atoms are shifted off the centers of the octahedral voids and form tetrahedral $M_4$ clusters with short metal−metal contacts. By means of band structure calculations on $GeV_4S_8$, we could show that the structure description $[M_4X_4]AX_4$ with strongly covalent bonded entities is more appropriate from the viewpoint of chemical bonding.[5]

The physical properties of $GaMo_4S_8$-type compounds have attracted much interest.[6−10] They are Mott insulators because of the long intercluster distances of about 4 Å. The electronic conduction is by hopping of carriers among the clusters, and $GaV_4S_8$ shows the behavior of a Fermi glass.[10] The localized electrons lead to magnetic properties when the cluster orbitals are partially filled. $GaMo_4S_8$ is ferromagnetic ($T_C = 26$ K) with one unpaired electron per cluster,[1] and $GeV_4S_8$ is antiferromagnetic with two unpaired electrons per $V_4$ unit ($T_N = 15$ K).[5] $GaV_4S_8$ was first reported by Brasen et al. in 1975 to be weakly magnetic,[6] but no evaluation of the magnetic data was given. Even no exact structural data of $GaV_4S_8$ are known. They are, however, an important prerequisite for reliable band structure calculations. A structural phase transition at low temperatures was expected for $GaV_4S_8$ due to a magnetic anomaly.[6] This low-temperature structure was not known up to now, and it was still assumed that this compound shows the same distortion as found in $GaMo_4S_8$.[11]

In the present paper we report single-crystal data of cubic $GaV_4S_8$ and the structure of the low-temperature modification derived from X-ray powder data. Detailed magnetic data are presented. Results of electronic band structure calculations for low-temperature $GaV_4S_8$ and $GaMo_4S_8$ are given in terms of band dispersions, and bonding interactions were analyzed by means of the COHP method. A simple orbital interacting scheme is

* E-mail: johrendt@uni-duesseldorf.de.
† E-mail: rapch@cup.uni-muenchen.de.

(1) Barz, H. *Mater. Res. Bull.* **1973**, *8*, 983.
(2) Perrin, C.; Chevrel, R.; Sergent, M. *J. Solid State Chem.* **1976**, *19*, 305.
(3) Perrin, C.; Chevrel, R.; Sergent, M. *C. R. Acad. Sci. Paris* **1975**, *C 280*, 949.
(4) Ben Yaich, H.; Jegaden, J. C.; Potel, M.; Sergent, M. *J. Less-Common Met.* **1984**, *102*, 22.
(5) Johrendt, D. *Z. Anorg. Allg. Chem.* **1998**, *624*, 952.
(6) Brasen, D.; Vandenberg, J. M.; Robbins, M.; Willens, R. H.; Reed, W. A.; Sherwood, R. C.; Pinder, X. J. *J. Solid State Chem.* **1975**, *13*, 298.
(7) Rastogi, A. K.; Wohlfarth, E. P. *Phys. Status Solidi* **1987**, *142*, 569.
(8) Shamrai, V. F.; Leitus, G. M. *Sov. Phys. Solid State* **1987**, *29*, 1312.
(9) Sahoo, Y.; Rastogi, A. K. *J. Phys.: Condens. Matter* **1993**, *5*, 5933.
(10) Rastogi, A. K.; Niazi, A. *Physica B* **1996**, *223 & 224*, 588.
(11) Francois, M.; Lengauer, W.; Yvon, K.; Ben Yaich-Aerrache, H.; Gougeon, P.; Potel, M.; Sergent, M. *Z. Kristallogr.* **1991**, *196*, 111.

10.1021/cm001099b CCC: $19.00 
Published on Web 09/07/2000

developed in order to explain the driving forces of the structural transitions.

## Experimental Section

Samples of $GaV_4S_8$ were prepared by heating of stoichiometric mixtures of the elements (purities > 99.5%) in quartz glass tubes under argon atmosphere. The samples were heated to 1073 K at the rate of 50 K/h for 1 day and furnace cooled to room temperature. After homogenization in an argon-filled glovebox, the samples were annealed at 1123 K for 15 h. This procedure yielded dark gray powders, which show no reaction when exposed to air or humidity. Small single crystals suitable for X-ray experiments show metallic luster.

X-ray powder experiments were performed with a Guinier diffractometer (Huber G644, Cu $K\alpha_1$, silicon as external standard) at room temperature and with a Bragg−Brentano diffractometer (Siemens D5000, Cu $K\alpha$), equipped with a helium evaporation cryostat at 20 K. Single-crystal intensity data were collected on an automated four-circle diffractometer (STOE AED-2, Mo $K\alpha$, graphite monochromator, $3° \le 2\theta \le 80°$). Structure refinements were performed with the Shelx97[12] package for single crystal data and with and the Rietveld least-squares program Wyriet[13] for low-temperature powder data. Additional material on the refinements is deposited.[14]

The electrical resistivity of $GaV_4S_8$ was measured on polycrystalline pellets (cold pressed with 50 kN, annealed at 1073 K for 15 h) using a four-probe dc current reversal technique[15] between 30 and 300 K. Magnetic susceptibilities of polycrystalline $GaV_4S_8$ were determined with a SQUID magnetometer (MPMS, Quantum Design, Inc.) between 2 and 300 K with magnetic flux densities up to 5.5 T.

Self-consistent band structure calculations were performed using the LMTO method in its scalar relativistic version (program LMTO-ASA 47c).[16] A detailed description may be found elsewhere.[17] Reciprocal space integrations were performed with the tetrahedron method using 120 irreducible *k* points within the trigonal Brillouin zones.[18] The basis sets consisted of 4s/4p for Ga, 3s/3p for S, 3d/4s/4p for V, and 4d/5s/5p for Mo. The 4d orbitals for Ga, 3d for S, and 4f for Mo were treated by the downfolding technique.[19] To achieve space filling within the atomic sphere approximation, interstitial spheres are introduced to avoid too large overlap of the atom-centered spheres. The empty sphere positions and radii were calculated using an automatic procedure developed by Krier et al.[20] We did not allow an overlap of more than 15% for any two atom-centered spheres. Owing to the magnetic properties, spin-polarized calculations were performed using the exchange-correlation potential by von Barth and Hedin.[21] To investigate chemical bonding in more detail, we have calculated the crystal orbital Hamiltonian population (COHP)[22] for selected bonds. COHP represents an energy-resolved bonding descriptor based on an energy-partitioning scheme in contrast to the well-known crystal orbital overlap population (COOP), which is an electron-partitioning scheme. Negative values for the COHP indicate bonding, while positive values indicate antibonding contributions. To make COHP diagrams similar to the COOP, we plot −COHP versus energy.

**Table 1. Crystal Data and Structure Refinement for *RT*-$GaV_4S_8$**

| | |
|---|---|
| data collection temp | 295 K |
| empirical formula | $GaV_4S_8$ |
| formula weight | 530.02 g/mol |
| space group | $F\bar{4}3m$ (No. 216) |
| lattice constant | $a = 9.661(1)$ Å |
| volume, formula units | 901.71 Å$^3$, $Z = 4$ |
| density, calc | 3.90 g cm$^{-3}$ |
| absorption coeff | $\mu$(Mo K$\alpha$) = 8.72 mm$^{-1}$ |
| diffractometer | STOE AED-2 |
| wavelength | 0.71069 Å |
| $\theta$ range | $3° \le 2\theta \le 80°$ |
| reflections collected | 1264 |
| independent reflections | 181 |
| twin ratio | 0.52(6) |
| $R_{(int)}$ | 0.031 |
| $R_1$ (all data) | 0.022 |
| $R_{w2}$ (all data) | 0.054 |

Atomic Positions and Isotropic Displacement Parameters (pm$^2$)

| | | | |
|---|---|---|---|
| Ga | 4*a* (*0,0,0*) | | $U = 64(3)$ |
| V | 16*e* (*x,x,x*) | $x = 0.6060(1)$ | $U = 68(2)$ |
| S1 | 16*e* (*x,x,x*) | $x = 0.3707(1)$ | $U = 81(3)$ |
| S2 | 16*e* (*x,x,x*) | $x = 0.8642(1)$ | $U = 71(4)$ |

Selected Interatomic Distances (Å)

| | | | |
|---|---|---|---|
| V−3 S1 | 2.295(2) | V−3 V | 2.896(2) |
| V−3 S2 | 2.528(1) | V−3 V | 3.936(3) |
| Ga−4 S2 | 2.272(2) | | |

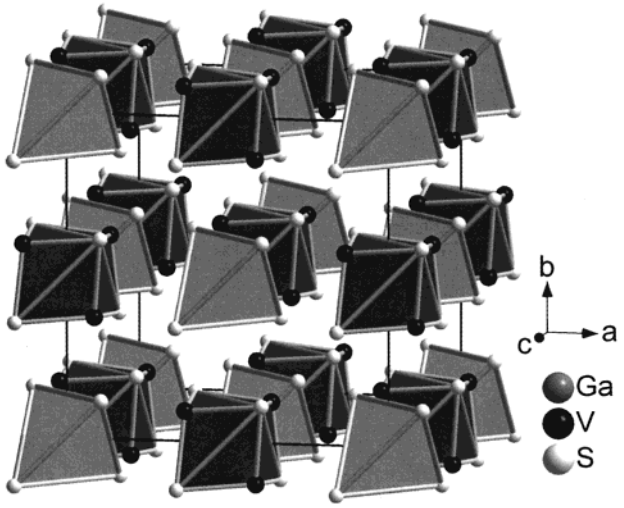


**Figure 1.** Crystal structure of $GaV_4S_8$. The NaCl-like arrangement of $V_4S_4$ cubes and $GaS_4$ tetrahedra is emphasized.

## Results and Discussion

**X-ray Diffraction.** Powder patterns of $GaV_4S_8$ could be indexed on the basis of a face-centered cubic lattice. Refinements of the lattice parameter give $a = 9.661(1)$ Å, in good agreement with previous investigations.[6] Single-crystal intensities were collected at room temperature and refined using the atomic positions of $GeV_4S_8$ as initial parameters. The final cycles were performed with regard to twin domains convertible by inversion. The results are summarized in Table 1, including selected interatomic distances. As expected, the single-crystal data confirm the $GaMo_4S_8$ structure at room temperature (*RT*-$GaV_4S_8$). Figure 1 emphasizes the NaCl-like arrangement of $[V_4S_4]$ heterocubane entities and $[GaS_4]$ tetrahedra. A more detailed description

(12) Sheldrick, G. M. *Shelxl-97, Programs for the Refinement of Crystal Structures;* Universität Göttingen: 1997.
(13) WYRIET, *Program for Rietveld Analysis, Vers. DBW9006, Rel. 8.4.91*; Shool of Physics, Georgia Institute of Technology: Atlanta, GA.
(14) Details can be obtained from Fachinformationszentrum Karlsruhe, D-76344 Eggenstein-Leopoldshafen (Germany), by quoting the Registry No's CSD-411315 (*RT*-$GaV_4S_8$) and CSD-411314 (*LT*-$GaV_4S_8$).
(15) Yeager, J., Hrusch-Tupta, M. A., Eds. *Low Level Measurements*; Keithley Instruments Inc.: Cleveland, OH, 1998.
(16) Andersen, O. K. *Tight-Binding LMTO 47*; Max-Planck-Institut für Festkörperforschung: Stuttgart, 1994.
(17) Skriver, H. L. *The LMTO Method*; Springer-Verlag: Berlin, 1984.
(18) Andersen, O. K.; Jepsen, O. *Solid State Commun.* **1971**, *9*, 1763.
(19) Lambrecht, W. R. L.; Andersen, O. K. *Phys. Rev. B* **1986**, *34*, 2439.
(20) Krier, G.; Jepsen, O.; Andersen, O. K. Unpublished.
(21) von Barth, U.; Hedin, L. J. *Phys. C: Solid State Phys.* **1982**, *5*, 1629.
(22) Dronskowski, R.; Blöchl, P. E. *J. Phys. Chem.* **1993**, *97*, 8617.

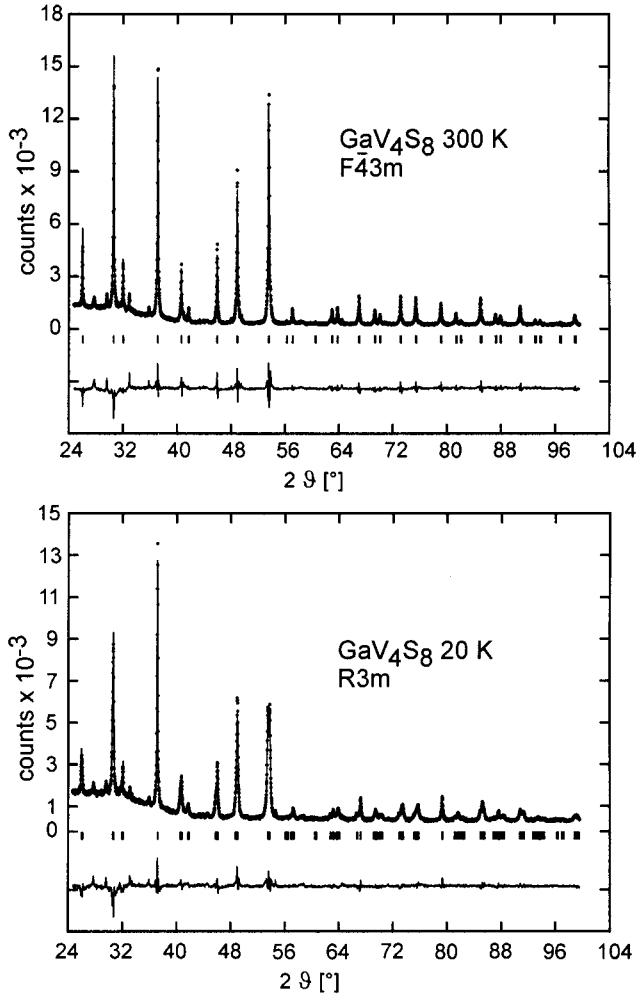


**Figure 2.** X-ray powder patterns and Rietveld fits of $GaV_4S_8$ at 300 K (top) and at 20 K (bottom).

of the structure is given elsewhere.[5] No indications for a disorder of the cation sites were detected. All positions are fully occupied, and we have found no residual electron density in the empty tetrahedral or octahedral voids. The intra- and intercluster V−V distances at room temperature are 2.896(2) and 3.936(3) Å, respectively, in contrast to the values given in ref 23.

A low-temperature phase transition as in $GaMo_4S_8$ was also supposed for $GaV_4S_8$ due to magnetic anomalies around 40 K.[6,23] We have recorded an X-ray powder pattern at 20 K. Several lines split or were broadened, indicating a lowering of symmetry. The unit cell at 20 K (*LT*-$GaV_4S_8$) is rhombohedral with $\alpha_{rh} = 59.66°$ in contrast to *LT*-$GaMo_4S_8$ with $\alpha_{rh} = 60.53°$.[11] This means the distortion from cubic *F* symmetry ($\alpha_{rh} = 60°$) in *LT*-$GaV_4S_8$ is of the same kind as in *LT*-$GaMo_4S_8$, but it runs in the opposite direction. The space group symmetry is reduced from $F\bar{4}3m$ to $R3m$ via a translationengleiche symmetry reduction of index 4 (t4). With the structural model of *LT*-$GaMo_4S_8$ we carried out the Rietveld profile fit shown in Figure 2. The final parameters, *R* values, and selected atomic distances are listed in Table 3. Attempts to refine the data with rhombohedral angles $\alpha_{rh} > 60°$ were not successful.

Even if the distortion from *RT*- to *LT*-$GaV_4S_8$ is small, it produces significant changes in the geometry of the

(23) Shanti, N.; Sarma, D. D. *J. Solid State Chem.* **1999**, *148*, 143.

**Table 2. Crystal Data and Structure Refinement for *LT*-$GaV_4S_8$**

| | |
|---|---|
| data collection temperature | 20 K |
| empirical formula | $GaV_4S_8$ |
| formula weight | 530.02 g/mol |
| space group | $R3m$ (No. 160) |
| lattice constants | $a = 6.799(1)$ Å, $c = 16.782(2)$ Å |
| | $a_{rh} = 6.834(1)$ Å, $\alpha_{rh} = 59.66(2)°$ |
| volume, formula units | 671.84 Å$^3$, $Z = 3$ |
| density, calc | 3.930 g cm$^{-3}$ |
| diffractometer | SIEMENS D5000 |
| wavelength | 1.5418 Å |
| range in $2\theta$ | $18° \le 2\theta \le 99.9°$ |
| step width | 0.02° |
| no. of Bragg reflections | 324 |
| profile function | pseudo-Voigt |
| halfwidth *u*,*v*,*w* | 0.55(3), −0.37(2), 0.081(5) |
| no. of variables | 16 |
| $R_p$, $R_{wp}$ | 0.070, 0.098 |
| $R_{Bragg(I)}$, $R_F$ | 0.066, 0.060 |

Atomic Positions

| | | *x* | *z* |
|---|---|---|---|
| Ga | 3*a* (*0,0,z*) | 0 | 0 (fixed) |
| V1 | 3*a* (*0,0,z*) | 0 | 0.3903(5) |
| V2 | 9*b* (*x,2x,z*) | 0.1943(5) | 0.2001(5) |
| S1 | 3*a* (*0,0,z*) | 0 | 0.6285(8) |
| S2 | 9*b* (*x,2x,z*) | 0.1686(8) | 0.4559(8) |
| S3 | 9*b* (*x,2x,z*) | 0.1827(7) | 0.9517(7) |
| S4 | 3*a* (*0,0,z*) | 0 | 0.1384(8) |

Selected Interatomic Distances (Å)

| | | | |
|---|---|---|---|
| V1−3 S2 | 2.270(8) | V2−1 S1 | 2.29(1) |
| V1−3 S3 | 2.50(1) | V2−2 S2 | 2.250(9) |
| V1−3 V2 | 2.90(1) | V2−2 S3 | 2.521(8) |
| Ga−3 S3 | 2.300(7) | V2−1 S4 | 2.511(7) |
| Ga−1 S4 | 2.32(1) | V2−2 V2 | 2.836(5) |

**Table 3. Metal−Metal Distances in $GaV_4S_8$ and $GaMo_4S_8$**

| | $GaV_4S_8$ (M = V) | | $GaMo_4S_8$ (M = Mo) | |
|---|---|---|---|---|
| | cubic | rhombohedral | cubic | rhombohedral |
| M1−3 M2 | 2.896(2) | 2.90(1) | 2.814(3) | 2.81(2) |
| M2−2 M2 | | 2.83(1) | | 2.89(1) |

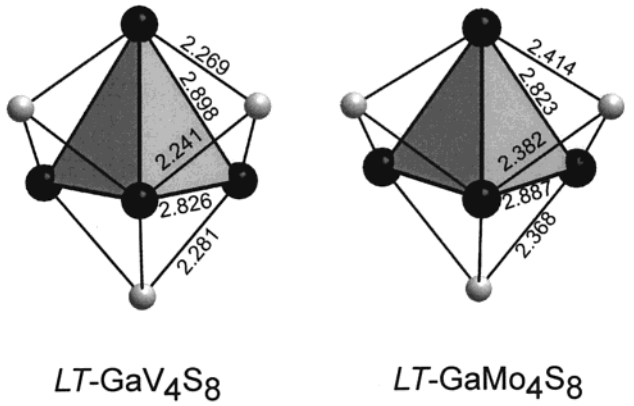


**Figure 3.** Distorted clusters of the low-temperature modifications of $GaV_4S_8$ (left) and $GaMo_4S_8$ (right). The distances are given in angstroms.

structure. The symmetry of all tetrahedral entities changes from $T_d$ to $C_{3v}$. Four Ga−S distances of 2.27 Å in the $GaS_4$ tetrahedron split into three times 2.29 Å and one times 2.32 Å, tantamount to an elongation along the 3-fold axis. In view of the magnetic and electronic properties, the changes within the $V_4$ cluster are most important. The differences in the cluster geometries of *RT*- and *LT*-$GaV_4S_8$ are depicted in Figure 3, and Table 3 shows the V−V distances in $GaV_4S_8$ compared with the Mo−Mo distances in $GaMo_4S_8$. We regard the $M_4$

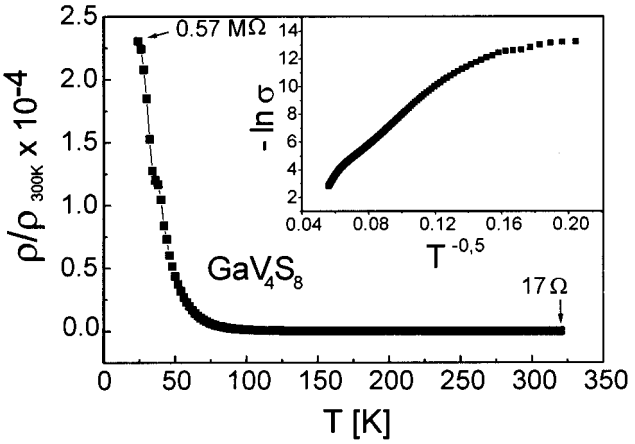


**Figure 4.** Electrical resistivity $\rho$ of $GaV_4S_8$ between 30 and 320 K. Inset: The VRH relation ln $\sigma$ versus $T^{-n}$ with $n = 1/2$.

(M = V, Mo) clusters built up by one M1 atom on the 3-fold axis lying over a triangle of three M2 atoms. In both cases the three M1−M2 distances remain nearly constant within experimental errors. But the three M2−M2 bonds within the plane shrink from 2.90 to 2.83 Å when M = V, whereas they expand from 2.81 to 2.89 in the case of M = Mo. Thus, we observe different changes of metal−metal bonding in the $V_4$ compared with the $Mo_4$ clusters during the phase transitions from cubic to rhombohedral symmetry.

**Electrical Conductivity.** Figure 4 shows the temperature dependence of the electrical resistivity between 30 and 320 K.

The exponential decrease of conductivity to lower temperatures indicates thermal activation of carriers. The anomaly in the $\rho(T)$ plot is reproducible and may be attributed to the structural distortion. The phase transition temperature is 38 ± 2 K. The Arrhenius plot is not linear and shows a decrease of the energy gap in going to lower temperatures. Using the almost linear part around room temperature, we get a gap about $E_a$ = 0.14 eV, in agreement with ref 9. In the insert of Figure 4 we have plotted the relation ln $\sigma$ versus $T^{-n}$ with $n = {}^1/_2$. This intrinsic behavior indicates variable range hopping (VRH) or multielectron hopping at low temperatures. The VRH mechanism of the conductivity in $GaV_4S_8$ was investigated in detail by Rastogi et al.[7,9] Although the cluster orbitals are only partially filled, the material is not metallic because the distances between the clusters are too large (about 4 Å) for direct interactions. This means the electrons are "frozen" in the cluster orbitals, and the compound was called a Fermi glass.

**Magnetism.** The inverse magnetic susceptibility of $GaV_4S_8$ between 2 and 300 K is presented in Figure 5. We observe no pure Curie−Weiss behavior but a slight downward curvature of $1/\chi(T)$. For this reason we have fitted the data with a small amount of a temperature-independent susceptibility contribution of $\chi_0 = 11 \times 10^{-9}$ $m^3$/mol and obtained a paramagnetic Curie temperature of $\theta$ = 3.7(1) K. Due to the nonlinear $1/\chi(T)$ plot, the effective magnetic moment per formula unit shows a temperature dependency ranging from 1.9$\mu_B$ at 300 K to 1.5$\mu_B$ at 50 K per formula unit, as depicted in the inset of Figure 5. This shows clearly the deviation from the Curie law, which may also result from the delocalization of electrons in cluster MO's. However, these values are compatible with one unpaired electron per $V_4$ cluster (theoretical value 1.73$\mu_B$) in $GaV_4S_8$. Ferromagnetic ordering is detected from the sharp bend in $1/\chi(T)$ at $T_C$ = 10 ± 1 K (inset in Figure 5). The magnetization curve at 2 K (Figure 6) shows nearly saturation against (0.80 ± 0.01)$\mu_B$ per formula unit at 5.5 T. The anomaly in the $1/\chi(T)$ plot discernible near 40 K may be attributed to the structural phase transition, in agreement with the resistivity measurement.

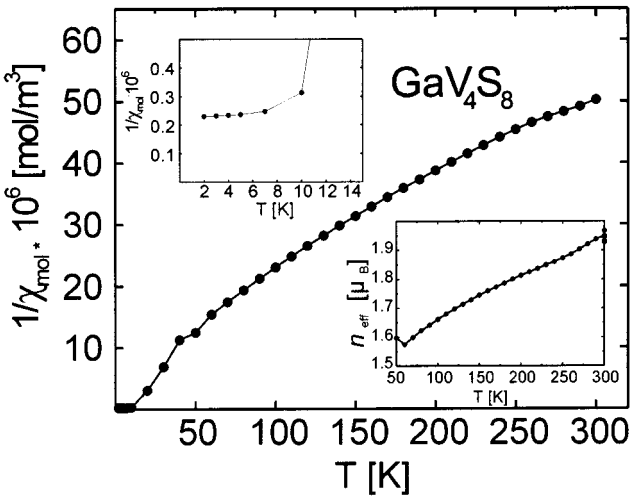


**Figure 5.** Temperature dependence of the inverse magnetic susceptibility of $GaV_4S_8$. Insets: $1/\chi(T)$ in the low-temperature range 2−14 K (top left) and the temperature dependence of the magnetic moment (bottom right).

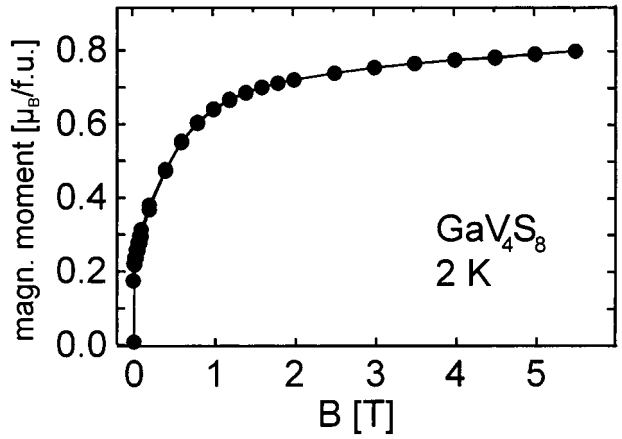


**Figure 6.** Magnetization versus the external field strength of $GaV_4S_8$ at 2 K.

**Electronic Structure.** From our crystallographic results two questions arise: (i) what are the driving forces for the phase transition, and (ii) why do the distortions occur in opposite directions for $GaV_4S_8$ and $GaMo_4S_8$? It is clear that the magnetic and transport properties of $GaMo_4S_8$-type compounds depend strongly on the electronic structure of the $M_4$ cluster. The first self-consistent band structure calculations on the closely related compound $GeV_4S_8$ showed very narrow bands near the Fermi level, and so electron−electron interactions play an important role.[5,23] The density of states (DOS) in this energy range is dominated by metal−metal bonding states of the $V_4$ cluster generated by the V 3d orbitals. In the cubic case, the symmetries of the cluster orbitals at Γ are $a_1$, $e$, and $t_2$. The latter one is

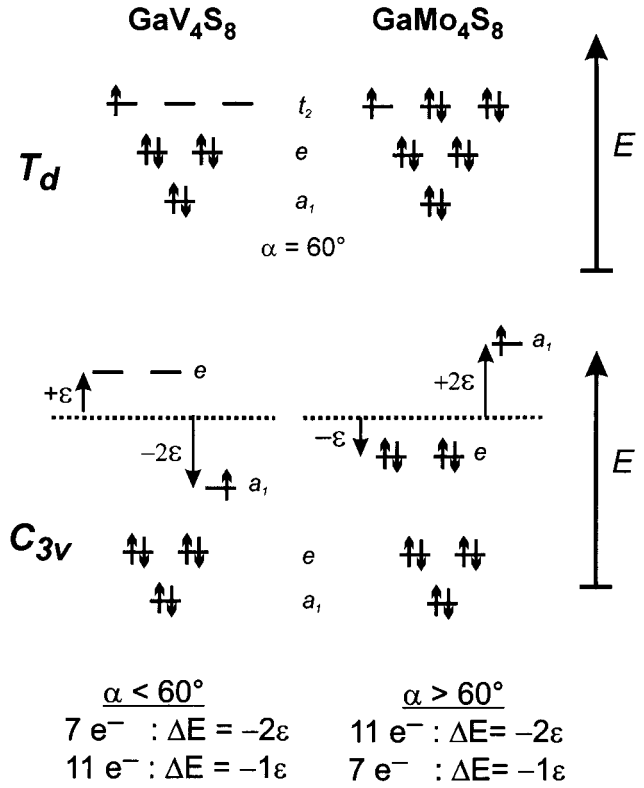


**Figure 7.** MO schemes of the cluster orbitals in $GaV_4S_8$ and $GaMo_4S_8$ for different rhombohedral angles $\alpha_{rh}$.

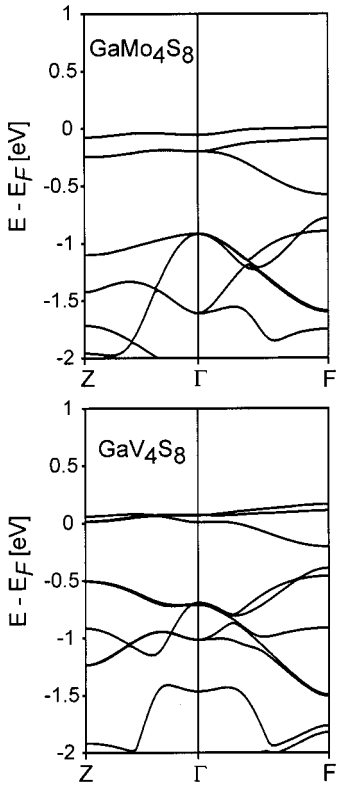


**Figure 8.** Band dispersions for the majority spin along two symmetry lines for $GaMo_4S_8$ (top) and $GaV_4S_8$ (bottom).

the highest occupied, 3-fold degenerated level. The cluster orbitals are completely filled with 12 electrons. According to the idealized ionic formula splitting $Ga^{3+}(V^{3.25+})_4(S^{2-})_8$ only seven electrons are available for metal−metal bonding in $GaV_4S_8$ but eleven are available in $GaMo_4S_8$. So the 3-fold degenerated highest level contains one electron in the vanadium and five in the molybdenum compound. In both cases one spin should remain unpaired, which is in agreement with the experimental magnetic moments. The structural distortion reduces the symmetry and removes the degeneracy of the $t_2$-level ($T_d$) by splitting it into a pair of degenerated levels with $e$ symmetry and one level with $a_1$ symmetry ($C_{3v}$). From this we can derive the MO schemes shown in Figure 7. In the case of ideal cubic symmetry ($\alpha_{rh} = 60°$), the 3-fold degenerated $t_2$ level is occupied by one or five electrons for $GaV_4S_8$ or $GaMo_4S_8$, respectively. When the rhombohedral angle $\alpha_{rh}$ changes, we get an opposing effect depending on whether $\alpha_{rh}$ gets smaller or larger than 60°. For $\alpha_{rh} < 60°$, the $a_1$ level ($C_{3v}$) is stabilized and the energy of the $e$ levels increases. But when $\alpha_{rh} > 60°$, the level splitting is reversed, the $a_1$ level goes up in energy, and the $e$ levels go down in energy, as shown schematically in Figure 7. The centers of gravity (dotted lines in Figure 7) with respect to the energy of the $t_2$ energy levels are not affected by the splitting. This means, when the $a_1$ level goes down by an energy amount $-2\epsilon$, the two $e$ levels must go up by $+1\epsilon$ and vice versa. Filling the MO's with 7 electrons, we get a stabilization of $-2\epsilon$ for $\alpha_{rh} < 60°$ and one of $-1\epsilon$ for $\alpha_{rh} > 60°$. This is reversed for 11 electrons to $-1\epsilon$ for $\alpha_{rh} < 60°$ and $-2\epsilon$ for $\alpha_{rh} > 60°$. It is clear now that the rhombohedral distortion in $GaV_4S_8$ is energetically favored toward smaller angles $\alpha_{rh}$, whereas the opposite is valid for $GaMo_4S_8$.

To confirm this simple model described above, we have calculated self-consistent spin polarized band structures of rhombohedral $GaV_4S_8$ using the structural data obtained from the X-ray experiments. For rhombohedral $GaMo_4S_8$ the geometry from ref 11 was used. Since some main features of the electronic structures are already known,[5,23] we focus our analysis on those parts of the band structure which are affected by the structural distortion. The spin polarized calculations result in magnetic moments according to one unpaired electron per $V_4$ and $Mo_4$ cluster, respectively, in excellent agreement with the experiments. Figure 8 shows the band dispersions of rhombohedral $GaV_4S_8$ and $GaMo_4S_8$ along the symmetry lines $Z(1/2,1/2,1/2) \rightarrow \Gamma$-$(0,0,0) \rightarrow F(1/2,1/2,0)$. Only the bands for the majority spin are shown for the sake of clarity. The band splittings as predicted by the MO scheme are clearly discernible near the Fermi level at Γ. In $GaMo_4S_8$, the 2-fold degenerate ($e$) levels are lower in energy compared with the nondegenerated ($a_1$) level, but the opposite is observed in $GaV_4S_8$. To understand why the $a_1$ levels are affected in such different ways by the rhombohedral angle $\alpha_{rh}$, we have analyzed the orbital eigenvectors at Γ. Due to the high symmetry, the orbital is quite simple and consists purely of $3d_{z^2}$ contributions from the cluster atoms, as depicted in Figure 9. This combination is bonding between the three metal atoms of the triangle plane of M2 atoms but antibonding with respect to the M1 atom on the 3-fold axis. When $\alpha_{rh}$ decreases and the tetrahedron gets elongated, the antibonding M1−M2 interaction decreases, whereas the bonding increases between the M2 atoms. Since in *LT*-$GaV_4S_8$ with seven cluster electrons the $a_1$ level is the highest occupied one, this structure is stabilized electronically for a rhombohedral angle smaller than 60°.

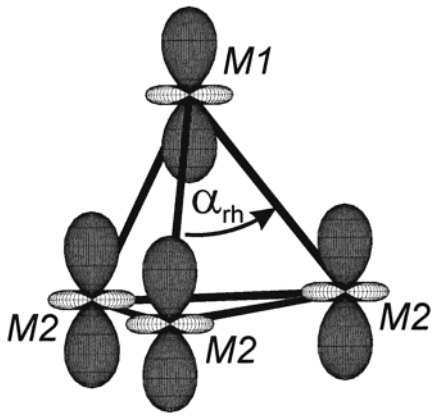


**Figure 9.** $a_1$ cluster MO for rhombohedral ($C_{3v}$) symmetry.

Conversely, the energy of the $a_1$ level increases for $\alpha_{rh} > 60$ because its antibonding character increases. In the case of *LT*-$GaMo_4S_8$ eleven electrons are available for the six cluster orbitals and almost all bonding states are filled. Now the distortion pushes up the antibonding $a_1$ level to the top of the band, and so it becomes only half filled. Thus, the $Mo_4$ cluster is likewise stabilized electronically, but for rhombohedral angles larger than 60°.

This local picture of orbital interactions remains valid even in the extended solid, because the intercluster distances are large in these compounds, which leads to very narrow bands at the Fermi level. The bonding character of the cluster orbitals can also be shown by the COHP calculated for the M1−M2 and M2−M2 bonds, shown in Figure 10. Below the Fermi energy almost all contributions are bonding and can be assigned to the cluster MO's in Figure 7. The metal−metal bonding levels in $GaMo_4S_8$ are more broadened (≈2 eV) and lower in energy than those in $GaV_4S_8$ (≈1.2 eV), indicating that the Mo−Mo interactions are stronger than the V−V ones. The regions near the Fermi energies origin from the $a_1$ and *e* levels, slightly broadened to bands (width ≈ 0.5 eV). Indeed the COHP curve for the M1−M2 bond in $GaV_4S_8$ (solid line in Figure 10, top) shows weakly antibonding contributions just below the Fermi energy, which corresponds to the $a_1$ level. The bonding states above $E_F$ belong to the *e* levels pushed up in energy. *LT*-$GaV_4S_8$ gets more stable than *RT*-$GaV_4S_8$ by the reduction of the antibonding M1−M2 interaction and a lowering of the highest occupied state, that is, the Fermi level. These antibonding $a_1$ states are also discernible in *LT*-$GaMo_4S_8$ (solid line in Figure 10, bottom). But now they are at the top of the band above the *e* levels and only partially filled, which stabilizes the $Mo_4$ cluster by reducing the M1−M2 antibonding interactions likewise and favoring the M2−M2 bonds. The COHP analysis confirms the mechanism of the electronic stabilization as suggested by the orbital scheme of Figure 7.

In summary, the low-temperature structural transitions in $GaV_4S_8$ and $GaMo_4S_8$ have a common origin in the electronic band structure. Orbital degeneracies, caused by the initially cubic symmetry, are removed in the sense of a Peierls distortion, and both structures

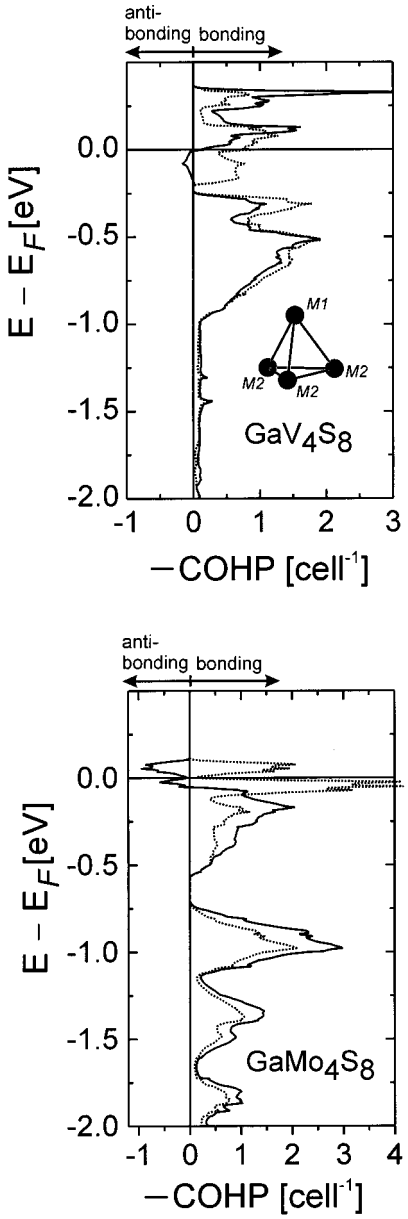


**Figure 10.** COHP diagrams (spin ↑ + spin ↓) for the M−M bonds in $GaV_4S_8$ (top) and $GaMo_4S_8$ (bottom): solid lines, M1−M2 bonds; dotted lines, M2−M2 bonds.

get stabilized electronically. But the striking feature is that the direction of the structural deformation is determined by particular orbital interactions within the tetrahedral clusters and depends on the number of electrons available for metal−metal bonding.

**Acknowledgment.** We thank Dr. C. Huhnt for the low-temperature X-ray measurements. Special thanks to Dipl.- Chem. G. Kotzyba and Prof. Dr. W. Jeitschko for the susceptibility measurement. We are indebted to Prof. Dr. A. Mewis and Prof. Dr. W. Frank for their interest and steady support of this work. This work was supported financially by the Deutsche Forschungsgemeinschaft and the Fonds der Chemischen Industrie.

CM001099B